^{57}Fe Mössbauer Spectra, Crystal Structure, and Spin-Crossover Behavior of [Fe(mbpN)(lut)]BPh_4

Yonezo MAEDA,* Yosuke NODA, Hiroki OSHIO,† and Yoshimasa TAKASHIMA
Department of Chemistry, Faculty of Science, Kyushu University, Hakozaki, Higashiku, Fukuoka 812
† Applied Molecular Science, Institute for Molecular Science, Myodaiji, Okazaki 444
(Received February 12, 1992)

A new spin-crossover complex [Fe(mbpN)(lut)]BPh_4 (H_2mbpN; *N,N'*-bis[(2-hydroxy-5-methylphenyl)phenylmethylene]-4-azaheptane-1,7-diamine and lut; 3,4-dimethylpyridine) is reported. The structure of this complex was determined at 293 K, and the temperature dependence of the ^{57}Fe Mössbauer spectra and magnetic susceptibilities was examined. The complex undergoes a faster spin-state interconversion than the lifetime of the ^{57}Fe excited state (1×10^{-7} s). More importantly, it has been found that the quadrupole splittings of the complex show the lowest value at intermediate spin-state transformations. This behavior is illustrated by a model in which the electric field gradient of the high-spin state has the opposite sign with that of the low-spin state. The monoclinic crystal of [Fe(mbpN)(lut)]BPh_4 is of space group $P2_1/a$, with a=14.664(5), b=37.269(4), c=10.061(5) Å, β=90.97(3)°, Z=4, and refinement to R=0.079 and R_W=0.084. The bond distances of Fe–O^{av} (1.912(5) Å), Fe–N_{imine}^{av} (2.080(6) Å), Fe–N_{amine} (2.141(6) Å), and Fe–$N_{pyridine}$ (2.145(6) Å) are close to the expected values for the high-spin species.

The spin-state interconverion rates have usually been estimated relative to the time scales associated with various spectroscopic techniques: e.g., $t=10^{-7}$ s for ^{57}Fe Mössbauer spectroscopy and $t=10^{-10}$ s for esr. Recently, the iron(III) dithiocarbamates[1] and some of the iron(III) complexes with N_4O_2 ligand atoms[2-4] have been shown to interconvert faster than the Mössbauer time scale. In these Mössbauer spectra a single doublet showing a mean electronic state between low- and high-spin states is observed. Linear decreases of the quadrupole splitting with increasing temperature are usually observed for spin-crossover complexes, due to an increase in the high-spin fraction. However, the minimum in the quadrupole splitting in the spin transition temperature range is expected for a complex in which the sign of the electric field gradient for the high-spin state is different from that for low-spin state in theoretical terms[5] and was observed for the iron complex of the 3-ethoxysalicylidene Schiff-base [Fe(3-OEt-SalAPA)$_2$]ClO_4·C_6H_6 reported by Hendrickson et al.[6] The minimum in the quadrupole splitting was observed at about 200 K for the complexes reported here; the data were compared with a model previously reported.[5] [Fe(mbpN)(im)]BPh_4 (H_2mbpN; *N,N'*-bis[2-hydroxy-5-methylphenyl)phenylmethylene]-4-azaheptane-1,7-diamine and im;imidazole) and [Fe(salten)(mpy)]BPh_4 (H_2salten; *N,N'*-bis[(2-hydroxyphenyl)methylene]-4-azaheptane-1,7-diamine and mpy; 4-methylpyridine) were prepared for references in this study.

Experimental

The Schiff-base ligand H_2mbpN was prepared using 2-hydroxy-5-methylbenzophenone, as described elsewhere.[7] A methanol solution of H_2mbpN (1 mmol) containing a small amount of 2,2-dimethoxypropane was added to a methanol solution of anhydrous iron(III) chloride (1 mmol); an anhydrous methanol solution of 3,4-lutidine (3 mmol) was then added. The mixed solution was refluxed for over 30 min, after

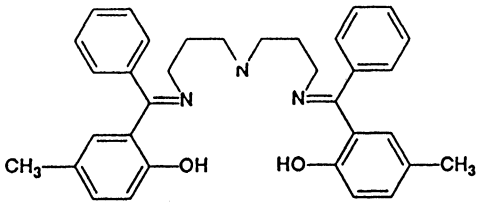

Schematic structure for H_2mbpN

which a methanol solution containing $NaBPh_4$ (2 mmol) was slowly added to the above mentioned solution. Dark-violet crystals were precipitated, filtered with a sintered-glass filter and washed with methanol. Since the precipitation contained much paramagnetic high-spin impurity in addition to the spin-crossover complexes, recrystallization was repeated five times from methanol. Tiny crystals which are dark-violet at room temperature and dark-green at 78 K were finally obtained. This type of color change of the crystals is usually observed for spin-crossover iron(III) complexes with Schiff-base ligands. Elemental analysis for [Fe(mbpN)(lut)]BPh_4: Found: C; 77.96, H; 6.51, N; 5.37, Fe; 5.53%. Calcd for $BC_{65}FeH_{64}N_4O_2$: C; 78.08, H, 6.45; N, 5.60; Fe; 5.59%. Elemental analysis for [Fe(mbpN)(im)]BPh_4: Found: C; 75.85, H; 6.06, N, 7.00, Fe; 5.78%. Calcd for $BC_{61}FeH_{59}N_5O_2$: C; 76.25, H; 6.09, N; 7.30, Fe; 5.71%. [Fe(mbpN)(im)]BPh_4 shows spin-crossover behavior only in appropriate solvent.

Complexes which contain pyridine or imidazole in terms of 3,4-lutidine as an apical ligand, and other salts, i.e. PF_6^-, ClO_4^-, and BF_4^- salts, were not crystallized, except for the complexes described here. It is reported that a "crystallographic hole" exists in the lattices of metal mbpN compounds which can accommodate whatever solvents are present during crystallization.[7] However, no solvents were contained in the complexes prepared here.

The Mössbauer and esr spectrometers, as well as measurement of the magnetic susceptibilities, are described elsewhere.[8] All Mössbauer spectra were fitted to Lorentzian line shapes using a least-squares method to obtain the absorption positions at the Computer Center of Kyushu University. Although it is not appropriate to fit the spectra to

a Lorentzian line shape for the sake of strong relaxation phenomena, it is permissible to make a fitting to determine the absorption positions. The isomer shifts are reported with respect to the centroid of the spectrum of iron foil enriched with ^{57}Fe at 296 K.

Crystal Structure Determination. Suitable single crystals were obtained by slow evaporation of acetone at 4°C.

Crystal Data. $BC_{65}FeH_{64}N_4O_2$, M=999.9, monoclinic, space group $P2_1/a$, Z=4, a=14.664(5), b=37.269(4), c=10.061(5) Å, β=90.97(3)°, V=5498(1) Å^3, λ=0.71073 Å, D_c=1.440 and D_o=1.41 g cm^{-3}, dark-purple, crystal dimensions: 0.2×0.3×0.3 mm.

Data Collection and Processing. Diffraction data were collected at 293 K on a Rigaku AFC5 four-circle diffractometer using the ω scan technique; graphite monochromated Mo $K\alpha$ radiation; 12611 reflections measured($0<h<19$, $0<k<48$, $-13<l<13$), 5590 independent data with $|F_o|>3\sigma(F_o)$. The intensities of the three standard reflections were monitored every 100 reflections, showing no greater fluctuations during data collection than that expected from Poisson statistics. Although intensity data were corrected for both Lorentz and polarization factors, they were not for absorption and extinction.

Structure Analysis and Refinement. The structure was solved by the conventional heavy-atom method and refined by a block-diagonal least-squares method with anisotropic thermal parameters for non-hydrogen atoms and isotropic for hydrogen atoms. A weighting scheme $w=[\sigma_c^2+(0.015|F_o|)^2]^{-1}$ was employed, in which σ_c was estimated from the counting statistics. The final indices (R and R_w) were 7.9 and 8.4%, respectively, which are defined as $R=(|F_o|-|F_c|)/\Sigma|F_o|$ and $R_w=[\Sigma w(|F_o|-|F_c|)^2/\Sigma w|F_o|^2]^{1/2}$. The atomic scattering factors for non-hydrogen atoms were taken from Ref. 9, and those for hydrogen atoms from Stewart et al.[10] The effects of anomalous scattering for non-hydrogen atoms were corrected for in structure factor calculations. A determination of the structural parameters was carried out with the universal Crystallographic Computation Program System UNICS III,[11] using a HITAC M-680 Computer at the Computer Center of Institute for Molecular Science. The final atomic coordinates for the cation and boron are given in Table 1.

Results and Discussion

Crystal Structure. The crystal structure of [Fe(mbpN)(lut)]BPh$_4$ was determined at 293 K; interatomic distances and bond angles for the cation are listed in Tables 2 and 3, respectively. The steric structure and numbering system for the cation are given in Fig. 1 using ORTEP.[12] The coordination sphere around the iron atom in the cation is approximately octahedral, with the two terminal oxygen atoms being *trans* to each other. The iron-lignad bond lengths of Fe–O^{av}, Fe–N$_{imine}^{av}$, Fe–N$_{amine}$, and Fe–N$_{pyridine}$ are 1.912(5), 2.080(6), 2.141(6), and 2.145(6) Å, respectively. These bond lengths are close to the average values for high-spin complexes.[8] This coordination geometry is similar to that for [Fe(salten)(mpy)]BPh$_4$, which is in an almost low-spin state (μ_{eff}=3.54 B.M. at 300 K),[13] except that the ligand configuration of the mbpN complex is (a) and that of the salten complex (b). The bond lengths for the mbpN complex are δ_{Fe-N}^{av}=0.107 Å and δ_{Fe-O}^{av} =0.03 Å, longer than those for the salten; the average deviations of the three bond angles of L–Fe–L′ from 180°

Table 1. Positional Parameters and Isotropic Displacement Parameters for All Atoms Except Hydrogen Atoms of the Cation and Boron Atom of [Fe(mbpN)(lut)]BPh$_4$ with Estimated Standard Deviations in Parentheses

Atom	x	y	z	U	Atom	x	y	z	U
Fe	0.53180(7)	0.61898(3)	0.52171(10)	0.0400(3)	C(19)	0.4512(5)	0.7131(2)	0.3428(8)	0.062(3)
O(1)	0.5494(3)	0.5830(1)	0.6555(5)	0.048(2)	C(20)	0.4442(6)	0.7494(2)	0.3687(8)	0.065(3)
O(2)	0.5104(3)	0.6562(1)	0.3946(4)	0.051(2)	C(21)	0.4947(6)	0.7656(2)	0.4733(8)	0.061(3)
N(1)	0.4239(4)	0.6410(2)	0.6377(6)	0.049(2)	C(22)	0.5522(5)	0.7443(2)	0.5497(7)	0.054(3)
N(2)	0.6324(4)	0.5975(2)	0.3921(6)	0.048(2)	C(23)	0.5601(5)	0.7068(2)	0.5269(7)	0.049(2)
N(3)	0.4387(4)	0.5835(2)	0.4333(5)	0.055(2)	C(24)	0.4860(7)	0.8057(2)	0.5021(10)	0.079(4)
N(4)	0.6322(4)	0.6520(2)	0.6018(6)	0.049(2)	C(25)	0.6294(5)	0.6864(2)	0.6045(7)	0.047(2)
C(1)	0.4843(5)	0.5631(2)	0.7074(7)	0.043(2)	C(26)	0.6983(5)	0.7081(2)	0.6816(7)	0.052(3)
C(2)	0.4945(5)	0.5529(2)	0.8421(7)	0.054(3)	C(27)	0.7614(5)	0.7293(2)	0.6176(9)	0.066(3)
C(3)	0.4283(5)	0.5325(2)	0.9032(7)	0.055(3)	C(28)	0.8279(6)	0.7478(3)	0.6939(10)	0.083(4)
C(4)	0.3504(5)	0.5208(2)	0.8348(7)	0.051(3)	C(29)	0.8284(7)	0.7443(3)	0.8316(10)	0.095(4)
C(5)	0.3399(5)	0.5299(2)	0.7018(6)	0.045(2)	C(30)	0.7656(8)	0.7237(3)	0.8957(10)	0.096(4)
C(6)	0.4058(4)	0.5513(2)	0.6356(6)	0.039(2)	C(31)	0.6977(7)	0.7053(2)	0.8211(8)	0.077(4)
C(7)	0.2777(6)	0.4988(3)	0.9070(8)	0.070(3)	C(32)	0.7134(5)	0.6319(2)	0.6567(8)	0.059(3)
C(8)	0.3929(4)	0.5591(2)	0.4934(6)	0.039(2)	C(33)	0.7661(5)	0.6175(3)	0.5337(9)	0.072(3)
C(9)	0.3251(5)	0.5368(2)	0.4176(6)	0.042(2)	C(34)	0.7209(5)	0.5870(2)	0.4570(9)	0.070(3)
C(10)	0.3507(5)	0.5039(2)	0.3653(7)	0.056(3)	C(35)	0.4286(6)	0.6431(2)	0.7714(8)	0.064(3)
C(11)	0.2863(6)	0.4841(2)	0.2889(8)	0.065(3)	C(36)	0.3552(6)	0.6531(2)	0.8495(8)	0.069(3)
C(12)	0.1998(5)	0.4969(2)	0.2658(8)	0.060(3)	C(37)	0.2729(6)	0.6625(2)	0.7835(9)	0.073(3)
C(13)	0.1751(5)	0.5294(2)	0.3190(8)	0.068(3)	C(38)	0.2685(6)	0.6607(2)	0.6431(8)	0.070(3)
C(14)	0.2373(5)	0.5502(2)	0.3952(8)	0.056(3)	C(39)	0.3440(6)	0.6498(2)	0.5759(8)	0.063(3)
C(15)	0.4326(6)	0.5871(2)	0.2854(7)	0.062(3)	C(40)	0.3665(9)	0.6537(3)	0.9994(9)	0.122(6)
C(16)	0.5203(7)	0.5729(3)	0.2239(8)	0.097(4)	C(41)	0.1889(7)	0.6744(3)	0.8611(10)	0.092(4)
C(17)	0.6009(6)	0.5657(3)	0.3135(9)	0.083(4)	B	0.9629(5)	0.6159(2)	0.0981(8)	0.047(3)
C(18)	0.5076(5)	0.6907(2)	0.4228(7)	0.048(2)					

Table 2. Interatomic Distance (Å) for the Cation of [Fe(mbpN)(lut)]BPh4 with Estimated Standard Deviations in Parentheses

Fe–O(1)	1.915(5)	Fe–O(2)	1.909(5)
Fe–N(1)	2.145(6)	Fe–N(2)	2.141(6)
Fe–N(3)	2.089(6)	Fe–N(4)	2.071(6)
O(1)–C(1)	1.322(8)	O(2)–C(18)	1.317(9)
N(1)–C(35)	1.348(10)	N(1)–C(39)	1.356(10)
N(2)–C(17)	1.495(11)	N(2)–C(34)	1.495(10)
N(3)–C(8)	1.286(8)	N(3)–C(15)	1.495(9)
N(4)–C(25)	1.281(9)	N(4)–C(32)	1.504(10)
C(1)–C(2)	1.413(10)	C(1)–C(6)	1.420(9)
C(2)–C(3)	1.385(11)	C(3)–C(4)	1.394(10)
C(4)–C(5)	1.387(9)	C(4)–C(7)	1.537(11)
C(5)–C(6)	1.426(9)	C(6)–C(8)	1.469(9)
C(8)–C(9)	1.496(9)	C(9)–C(10)	1.388(10)
C(9)–C(14)	1.396(10)	C(10)–C(11)	1.417(11)
C(11)–C(12)	1.373(12)	C(12)–C(13)	1.376(12)
C(13)–C(14)	1.414(11)	C(15)–C(16)	1.531(13)
C(16)–C(17)	1.499(13)	C(18)–C(19)	1.417(11)
C(18)–C(23)	1.422(10)	C(19)–C(20)	1.384(12)
C(20)–C(21)	1.412(11)	C(21)–C(22)	1.382(11)
C(21)–C(24)	1.528(11)	C(22)–C(23)	1.421(10)
C(23)–C(25)	1.483(10)	C(25)–C(26)	1.501(10)
C(26)–C(27)	1.383(11)	C(26)–C(31)	1.409(11)
C(27)–C(28)	1.410(13)	C(28)–C(29)	1.391(15)
C(29)–C(30)	1.369(15)	C(30)–C(31)	1.414(14)
C(32)–C(33)	1.565(12)	C(33)–C(34)	1.519(13)
C(35)–C(36)	1.395(12)	C(36)–C(37)	1.412(12)
C(36)–C(40)	1.515(12)	C(37)–C(38)	1.414(13)
C(37)–C(41)	1.534(13)	C(38)–C(39)	1.369(12)

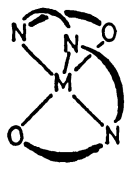

(a)

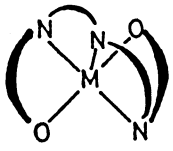

(b)

for the mbpN complex are 1.8° larger than that for the salten complex. The basal plane defined by Fe, O(1), O(2), N(3), and N(4) assumes a slight tetrahedral distortion, the deviations of the constituent atoms from the least-squares plane FeO_2N_2 being from 0.06 to −0.07 Å; the dihedral angle between the Fe–O(1)–N(3) and Fe–O(2)–N(4) planes is 5.5°. Two salicylideneaminato moieties produce a 'shallow' cave (or 'bow' shape), in which the lut ligand is positioned; the depth of the cave can be estimated (by the atom deviations from the FeO_2N_2 basal plane) to be 2.25 Å for C(4) and 2.35 Å for C(21). The dihedral angle between the two benzene rings of the two salicylideneiminato-moieties is 113.4°. The dihedral angle between the 3,4-lut plane and the FeO_2N_2 basal plane is 81.9°. The projection of the 3,4-lut plane onto the FeO_2N_2 basal plane makes an angle of 42.9° with the O(1)–Fe–N(1) plane, and the 3,4-lut plane bisects angle O(1)–Fe–N(4).

Magnetic Susceptibilities. The magnetic moments of [Fe(mbpN)(lut)]BPh4 vs. temperature are drawn in Fig.

Table 3. Bond Angles (°) for the Cation of [Fe(mbpN)(lut)]BPh4 with Estimated Standard Deviations in Parentheses

O(1)–Fe–O(2)	177.1(2)	O(1)–Fe–N(1)	88.7(2)
O(1)–Fe–N(2)	94.6(2)	O(1)–Fe–N(3)	86.3(2)
O(1)–Fe–N(4)	93.2(2)	O(2)–Fe–N(1)	88.4(2)
O(2)–Fe–N(2)	88.3(2)	O(2)–Fe–N(3)	94.4(2)
O(2)–Fe–N(4)	86.4(2)	N(1)–Fe–N(2)	175.4(2)
N(1)–Fe–N(3)	89.5(2)	N(1)–Fe–N(4)	95.0(2)
N(2)–Fe–N(3)	87.5(2)	N(2)–Fe–N(4)	88.1(2)
N(3)–Fe–N(4)	175.5(2)	Fe–N(1)–C(35)	122.6(5)
Fe–N(1)–C(39)	118.8(5)	Fe–N(2)–C(17)	114.1(5)
Fe–N(2)–C(34)	115.7(5)	Fe–O(1)–C(1)	125.5(4)
Fe–O(2)–C(18)	124.7(4)	Fe–N(3)–C(8)	126.1(4)
Fe–N(3)–C(15)	113.2(5)	C(8)–N(3)–C(15)	120.7(6)
C(17)–N(2)–C(34)	106.4(6)	Fe–N(4)–C(25)	125.4(5)
Fe–N(4)–C(32)	113.6(4)	C(25)–N(4)–C(32)	121.0(6)
O(1)–C(1)–C(2)	117.7(6)	O(1)–C(1)–C(6)	123.9(6)
C(2)–C(1)–C(6)	118.4(6)	C(1)–C(2)–C(3)	120.7(7)
C(2)–C(3)–C(4)	121.8(7)	C(3)–C(4)–C(5)	118.5(7)
C(3)–C(4)–C(7)	120.2(6)	C(5)–C(4)–C(7)	121.3(6)
C(4)–C(5)–C(6)	121.5(6)	C(1)–C(6)–C(5)	119.1(6)
C(1)–C(6)–C(8)	121.6(6)	C(5)–C(6)–C(8)	119.3(6)
N(3)–C(8)–C(6)	122.6(6)	N(3)–C(8)–C(9)	120.1(6)
C(6)–C(8)–C(9)	117.3(6)	C(8)–C(9)–C(10)	120.2(6)
C(8)–C(9)–C(14)	119.0(6)	C(10)–C(9)–C(14)	120.7(7)
C(9)–C(10)–C(11)	119.0(7)	C(10)–C(11)–C(12)	121.0(7)
C(11)–C(12)–C(13)	119.3(7)	C(12)–C(13)–C(14)	121.5(7)
C(9)–C(14)–C(13)	118.4(7)	N(3)–C(15)–C(16)	109.6(6)
C(15)–C(16)–C(17)	118.5(7)	N(2)–C(17)–C(16)	114.2(7)
O(2)–C(18)–C(19)	118.2(6)	O(2)–C(18)–C(23)	123.6(6)
C(19)–C(18)–C(23)	118.2(7)	C(18)–C(19)–C(20)	120.9(7)
C(19)–C(20)–C(21)	121.3(7)	C(20)–C(21)–C(22)	118.5(7)
O(20)–C(21)–C(24)	121.0(7)	C(22)–C(21)–C(24)	120.6(7)
C(21)–C(22)–C(23)	121.7(7)	C(18)–C(23)–C(22)	119.5(6)
C(18)–C(23)–C(25)	121.8(6)	C(22)–C(23)–C(25)	118.5(6)
N(4)–C(25)–C(23)	121.7(6)	N(4)–C(25)–C(26)	122.0(6)
C(23)–C(25)–C(26)	116.3(6)	C(25)–C(26)–C(27)	121.2(7)
C(25)–C(26)–C(31)	117.3(7)	C(27)–C(26)–C(31)	121.5(7)
C(26)–C(27)–C(28)	119.2(8)	C(27)–C(28)–C(29)	119.2(9)
C(28)–C(29)–C(30)	122.0(9)	C(29)–C(30)–C(31)	119.7(9)
C(26)–C(31)–C(30)	118.4(8)	N(4)–C(32)–C(33)	106.3(6)
C(32)–C(33)–C(34)	116.2(7)	N(2)–C(34)–C(33)	113.2(7)
C(35)–N(1)–C(39)	118.2(7)	N(1)–C(35)–C(36)	123.4(7)
C(35)–C(36)–C(37)	117.7(8)	C(35)–C(36)–C(40)	119.4(9)
C(37)–C(36)–C(40)	122.9(9)	C(36)–C(37)–C(38)	118.8(8)
C(36)–C(37)–C(41)	121.3(8)	C(38)–C(37)–C(41)	120.0(8)
C(37)–C(38)–C(39)	119.0(8)	N(1)–C(39)–C(38)	123.0(7)

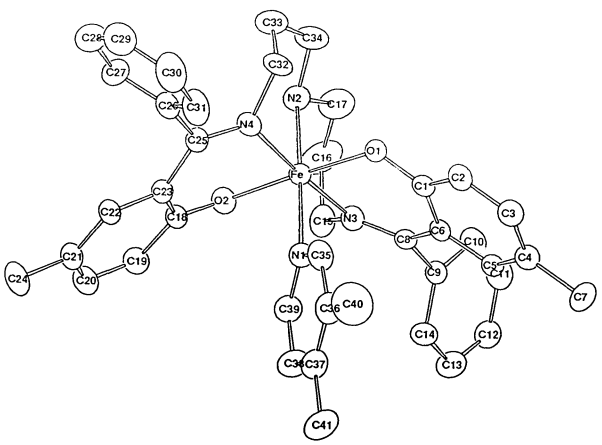

Fig. 1. Ortep figure for a $[Fe(mbpN)(lut)]^+$ cation.

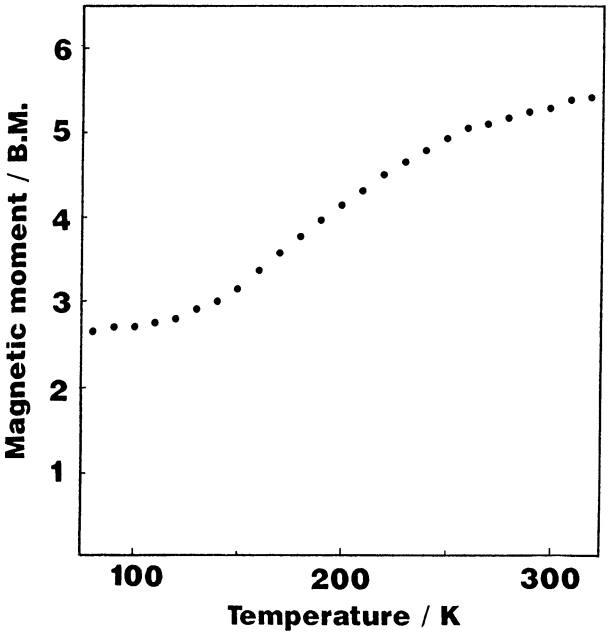

Fig. 2. Temperature dependence of the magnetic moments for [Fe(mbpN)(lut)]BPh_4.

2. The value of magnetic moment at 78 K, 2.64 B.M. is slightly larger than that characteristic of low-spin iron(III) compounds, and the value at 320 K, 5.40 B.M. is slightly lower than that characteristic of high-spin iron(III). The Mössbauer spectrum was therefore also measured at 4.2 K in order to estimate the amount of paramagnetic high-spin impurity; the amount was estimated to be approximately 7% from the area ratio of the Mössbauer absorption. (The spectrum is deposited as Fig. 8 in the supplemental materials.)

The values of the magnetic moments, for which the contribution due to the impurities(the impurity is supposed to be the other polymorphism of the spin-crossover complex and the magnetic moment was assumed to be 5.92 B.M.) was removed from the observed magnetic susceptibilities, were used to esimate the high-spin population of the spin-crossover complexes. If we suppose that the magnetic moments for the low- and high-spin states of the complex are μ_{ls}=2.05 and μ_{hs}=5.70 B.M., respectively, the high-spin population (x) at an arbitrary temperature can be estimated from

$$\mu^2 = x\mu_{hs}^2 + (1-x)\mu_{ls}^2.$$

The x value will be used later.

ESR Spectrum. Although an esr experiment for [Fe(mbpN)(lut)]BPh_4 was carried out for the solid and an acetone solution at 296 and 78 K, no signal was observed, even at 78 K, except for a broad signal (g=3.2) due to a paramagnetic impurity. The spectrum for [Fe(mbpN)(im)]BPh_4 in acetone at 296 K showed a broad line due to high-spin state at g=4.2. The spectrum at 78 K is shown in Fig. 3; the observed g-tensor components (g_{xx}=−1.822, g_{yy}=1.536, and g_{zz}=−3.219) were analyzed by the methods of Bohan.[14] Six eigenstates for Kramers doublets used were as follows:

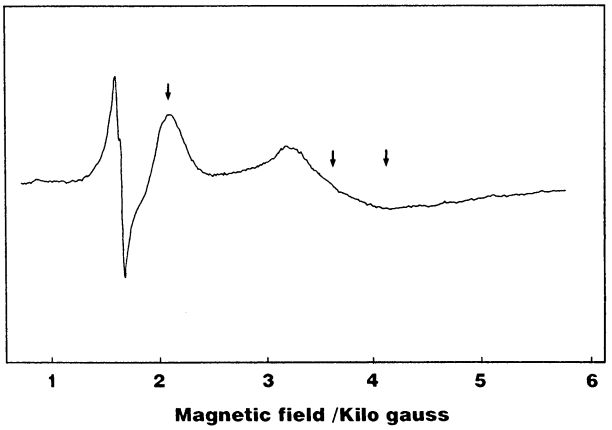

Fig. 3. ESR spectrum for [Fe(mbpN)(im)]BPh_4 in acetone.

$$\Psi_i^+ = A_i|+1,\alpha> + B_i|\zeta,\beta> + C_i|-1,\alpha> \qquad i=1,2,3 \text{ and}$$

$$\Psi_i^- = A_i|-1,\beta> - B_i|\zeta,\alpha> + C_i|+1,\beta> \qquad i=1,2,3.$$

This analysis indicates that an unpaired electron resides in the d_{zx} orbital (A=0.9022, B=0.0645, C=−0.4430, k=1.03, E_{ax}=10.45λ, E_{rhom}=1.40λ, $E1$=−4.38λ, $E2$=−2.61λ, $E3$=6.92λ), where λ is the spin-orbit coupling constant, k is orbital reduction factor, E_{ax} is the axial ligand field distortion parameter, and E_{rhom} gauges the rhombic distortion. The first excited state is d_{yz}, with an energy level of 1.77λ higher than the ground state. If λ is 460 cm^{-1} (this value is the maximum value, and is thus usually less for complexes),[15] the energy difference is 814 cm^{-1} or less. The esr spectrum of [Fe(salten)(mpy)]BPh_4 shows three well resolved signals at 78 K; g_{xx}=−2.095, g_{yy}=1.797, g_{zz}=−2.922 and g=4.4 (for high-spin species). The unpaired electron resides in the d_{zx} orbital (A=0.8337, B=0.0536, and C=−0.5533). These facts support the proposition that the electronic ground states of the low-spin isomers of both complexes are the same as each other, though the ground state of [Fe(mbpN)(lut)]BPh_4 is not decisive.

Mössbauer Spectra. Variable temperature Mössbauer spectra for [Fe(mbpN)(lut)]BPh_4 were measured, and are given in Fig. 4. The spectrum at 78 K shows a large quadrupole splitting that is characteristic of a low-spin iron(III) state. Ligand mbpN is pentadentate, and the coordination atmosphere of an iron atom is highly distorted from tetragonal symmetry. The spectra exhibit marked line-width asymmetries at low temperature (78 K), due to the fact that the spin–spin and/or spin–lattice interaction(the iron–iron atom

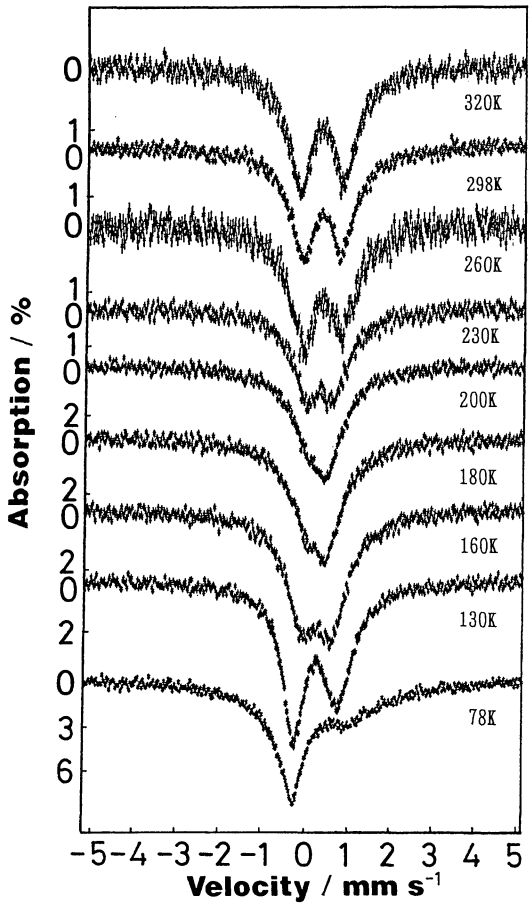

Fig. 4. Mössbauer spectra at various temperatures for [Fe(mbpN)(lut)]BPh4.

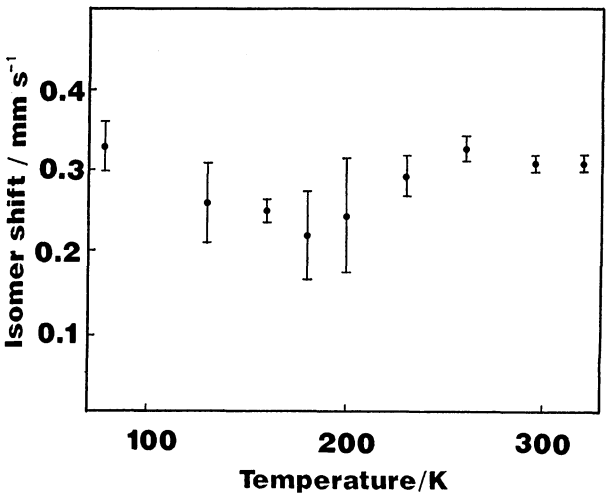

Fig. 5. Plots of the isomer shifts vs. the temperature for [Fe(mbpN)(lut)]BPh4.

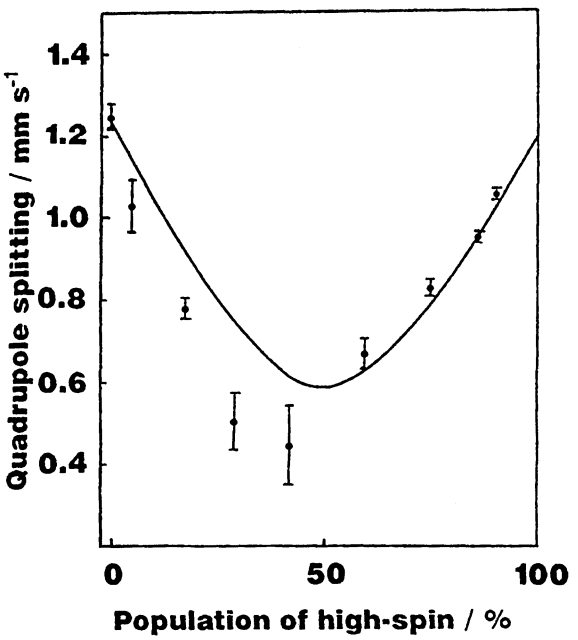

Fig. 6. Plots of the quadrupole splitting values vs. the high-spin fraction and a theoretical curve with ΔE_{ls}= 1.25 and ΔE_{hs}=−1.20 mm s^{-1}, and with interconversion rate of 10^8 s^{-1}. The bars indicate the standard deviations derived from a least-square calculation to obtain the parameters of the Mössbauer spectra.

distances are long, since the complex contains bulky ligands and anions). Line broadings of positive energy lines are also observed for [Fe(salten)(mpy)]BPh4 at 78 K. A plot of isomer shifts values vs. temperature observed (Fig. 5) supports the fact that the complexes are spin-crossover complexes; the decreases of the values with increasing temperature in the low- and high-temperature ranges are due to a second-order doppler shift of low- and high-spin states, respectively; the increase observed at between 200 and 280 K is due to an increase in the high-spin fraction.

It is concluded that the complexes undergo a fast spin-state interconversion between low- and high-spin states, a comparable to the Mössbauer lifetime, due to the fact that only a single doublet is observed in the spin-transition temperature range. The spectra were fitted to a single doublet with Lorentzian line shapes; the relevant quadrupole splitting values are plotted in Fig. 6 vs. the high-spin population (x) estimated from data concerning the magnetic moments. A plot of the values of the observed quadrupole splitting has a minimum at 200 K.

The origin of the electric field gradient (efg) tensors is different between the low- and high-spin states. For the low-spin state, the efg tensor results primarily from an asymmetric contribution of the valence electrons. This contribution to the efg can be temperature dependent via excitations to low-lying empty orbitals. In the high-spin case, the valence efg contribution is negligible, and the efg origin is largely due to lattice charges surrounding the ^{57}Fe nucleus. This may be temperature-dependent, especially if lattice expansion with temperature is not isotropic.

We pointed out that the existence of a minimum

quadruple splitting for complexes with fast spin-state interconversion is expected at some population ratio of low-spin to high-spin if the signs of the efg are different between the low- and high-spin states.[5] The Hamiltonian for a nucleus in an efg which jumps at random between high- and low-spin states can be written as,

$$H = H_0 + 1/2[(1+f(t))Q_{ls}](3I_z^2 - I^2) + 1/2[(1-f(t))Q_{hs}](3I_x^2 - I^2),$$

where H_0 is the Hamiltonian for a nucleus in the absence of any perturbations. Q_{ls} and Q_{hs} are $1/6\Delta E_{ls}$ and $1/6\ \Delta E_{hs}$, respectively, where ΔE_{ls} and ΔE_{hs} are the quadrupole splittings for the low- and high-spin states. Under the assumptions that the quadrupole splitting values of the low- and high-spin states are $+1.25$ and -1.20 mm s^{-1}, and that the interconversion rates between high- and low-spin states are 10^8 s^{-1}, the relaxation spectra calculated using the above mentioned Hamiltonian[5] are drawn in the Fig. 6; the spectra observed were analyzed by assuming a single doublet, the values of which are given in the figure. The solid line excellently agrees with the observed data, except that the plots are lower than the solid line in the large-population range of the low-spin state. One reason for this deviation is due to an increase in the population of the first excited state of the low-spin isomers, suggested from the esr result for [Fe(mbpN)(im)]BPh_4. On the other hand, the deviation of the angle of the principal-axis between q_{lat} and q_{val} from 90° results in a higher value than this theoretical curve, even though the model is based on many assumptions and uncertain values.

As was pointed out by Blume,[16] in cases where the spin–spin and/or spin–lattice relaxation times are not rapid relative to the ^{57}Fe nuclear Larmor precession frequency, intermediate paramagnetic relaxation broadens the $|I=1/2,\ M_I=\pm 1/2> \rightarrow |3/2,\ \pm 3/2>$ quadrupole component more than the $|1/2, \pm 1/2> \rightarrow |3/2, \pm 1/2>$ component. In this case, the signs of efg of the low-spin state of mbpN and salten complexes are positive in terms of the above discussion; a ^2E_g ground state is expected in accordance with the esr data.

On the other hand, the spectrum for the essentially high-spin state of [Fe(mbpN)(lut)]BPh_4 has almost a symmetric doublet, as is shown in the spectrum at 320 K. The sign of efg for the high-spin state can therefore not be estimated from the Mössbauer spectra. However, the crystal structures for the mbpN and salten complexes provide important information. Although the position of a BPh_4^- anion of the mbpN complex is located near to the *z*-axis, that of the salten complex is located on a plane defined by Fe, O(1), O(2), N(3), and N(4) (this plane is temporally taken as *xy* plane), as is shown in Fig. 7. The main axis of efg for a high-spin state of the salen complex would be near to the *xy* plane. It is probable that the main axis of efg for the mbpN complex changes from the *xy* plane to the *z*-axis direction, due to the electron density of the anion. The sign of q_{lat} of high-spin state for the mbpN complex is therefore different from that of the salen complex.

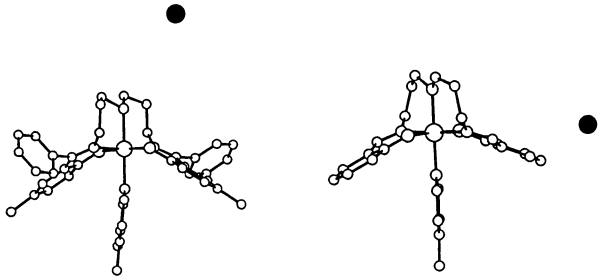

Fig. 7. Perspective drawings of [Fe(mbpN)(lut)]BPh_4 and [Fe(salten)(mpy)]BPh_4. The closed marks indicate the position of a boron atom as the center of a BPh_4^- anion.

Supplementary Materials are Available: The Mössbauer spectrum of [Fe(mbpN)(lut)]BPh_4 at 4.2 K (Fig. 8); tables of (1) crystal data and data collection; (2) the positional parameters and isotropic displacement parameters for all atoms, except for hydrogen atoms; (3) the mean-square displacement tensor for all atoms, except for hydrogen atoms; (4) the interatomic distance (Å) for the molecule; (5) the bond angles (°) for the molecule; and (6) the observed and calculated structure factors for [Fe(mbpN)(lut)]BPh_4 are deposited as Document No. 9008 at the Office of the Editor of Bull. Chem. Soc. Jpn.

References

1) G. R. Hall and D. N. Hendrickson, *Inorg. Chem.*, **15**, 607 (1976), and references cited therein.

2) W. D. Federer and D. N. Hendrickson, *Inorg. Chem.*, **23**, 3861 (1984); *ibid.*, **23**, 3870 (1984).

3) Y. Maeda, N. Tsutsumi, and Y. Takashima, *Inorg. Chem.*, **23**, 2440 (1984).

4) Y. Maeda and Y. Takashima, *Comments Inorg. Chem.*, **7**, 41 (1988).

5) Y. Maeda, Y. Takashima, N. Matsumoto, and A. Ohyoshi, *J. Chem. Soc., Dalton Trans.*, **1986**, 1115.

6) M. D. Timken, C. E. Strouse, S. M. Soltis, S. A. Daverio, D. N. Hendrickson, A. M. Adel-Mawgoud, and S. R. Wilson, *J. Am. Chem. Soc.*, **108**, 395 (1986).

7) P. C. Healy, G. M. Mockler, D. P. Freyberg, and E. Sinn, *J. Chem. Soc., Dalton Trans.*, **1975**, 691.

8) Y. Maeda, H. Oshio, K. Toriumi, and Y. Takashima, *J. Chem. Soc., Dalton Trans.*, **1991**, 1227.

9) J. A. Ibers and W. C. Hamilton, "International Tables for X-Ray Crystallography," Kynoch Press, Birmingham, England (1974), Vol. IV.

10) R. F. Stewart, E. R. Davidson, and W. T. Simpson, *J. Chem. Phys.*, **42**, 3175 (1965).

11) T. Sakurai and K. Kobayashi, *Sci. Rep. Inst. Chem. Phys. Res. Jpn.*, **55**, 69 (1979).

12) C. K. Johnson, ORTEP, Report ORNL-3794, Oak

Ridge National Laboratory, Oak Ridge, Tennessee (1965).
13) N. Matsumoto, S. Ohta, C. Yoshimura, A. Ohyoshi, S. Kohata, H. Okawa, and Y. Maeda, *J. Chem. Soc., Dalton Trans.*, **1985**, 2575.
14) T. L. Bohan, *J. Magn. Reson.*, **26**, 109 (1977).
15) B. N. Figgis, "Introduction to Ligand Fields," Interscience, New York (1966).
16) M. Blume, *Phys. Rev. Lett.*, **14**, 96 (1965).